International Journal for Housing Science and Its Applications
Publish August 10, 2025. Volume 46, Issue 4 Pages 5229-5241

https://doi.org/10.70517/ijhsa464363

Nonlinear dynamic optimization of a dual gyro stabilizer in complex sea conditions

Xinyu Gong[1,*], Siqi Mao[2] and Shixian Wu[1]
[1] Faculty of Shipping and Ship Engineering, Chongqing Jiaotong University, Chongqing, 400074, China
[2] Hohai College, Chongqing Jiaotong University, Chongqing, 400074, China
Corresponding authors: (e-mail: gongxinyu5925@163.com).

Abstract In the field of offshore engineering, the transverse rocking motion of ships in bad sea conditions seriously affects navigation safety and operation efficiency. The double gyroscope rocking reduction device provides a new idea for solving the ship stability problem under complex sea state by canceling the adverse effects of each other. In this paper, the optimization design method of double gyro rocking reduction device based on nonlinear dynamics equations is established for the transverse rocking problem of ships under complex sea conditions. Torsethaugen wave spectrum is used to simulate irregular wave conditions, a joint ship-gyro dynamic model is constructed, and a PD inlet controller based on transverse rocking angle feedback is designed. The damping coefficients of the rocking reduction gyro are optimized by genetic algorithm, and the fitness function with the rocking reduction efficiency and the degree of vibration shaking of the inlet damping as the objectives is established. The simulation results show that the optimized dual gyro shaking reduction system achieves a shaking reduction performance of about 90% under one-level wave conditions, which is improved to 80% compared with 72.22% before optimization. The multi-objective optimization increases the rocking reduction effect from 71.46% to 75.34%, and the rotor mass decreases from 2526 kg to 2165 kg. Adams dynamics simulation verifies that the device has a good rocking reduction effect in level 1-3 waves, but the rocking increase phenomenon may occur in high level waves. This study provides a theoretical basis and design method for the engineering application of double gyro rocking reduction device under complex sea conditions.

Index Terms Double gyro rocking reduction device, nonlinear dynamics, genetic algorithm, rocking reduction efficiency, inlet damping, multi-objective optimization

I. Introduction

For more than a hundred years, people have been devoted to the research of slowing down the ship's sway. Countries around the world have successively developed nearly one hundred different forms of rocking reduction devices, but at present, only rocking reduction tanks, bilge keels and rocking reduction fins are widely used, among which the rocking reduction fins are the monopoly, which have the best rocking reduction effect [1], [2].

In the process of sailing and working at sea, the ship will be affected by various factors such as waves, sea breeze and sea current, so the ship will produce various kinds of rocking such as transverse rocking, longitudinal rocking, transverse swinging, longitudinal swinging and so on [3]-[5]. The above irregular and violent swaying will seriously affect the safe navigation of the ship, the comfort of the passengers, and the normal work of various machines and equipments on board [6], [7]. Especially for military ships, the rocking of ships at sea can affect the normal takeoff, safe navigation and landing of airplanes [8], [9]. Therefore, tests and researches on ship rocking reduction have been the main work of technicians in the field of ships [10]. After years of research, it is found that the most widely used ship rocking reduction devices include the following, bilge keel, rocking reduction tank, rudder rocking reduction, rocking reduction fins, and integrated rocking reduction devices [11], [12]. However, in complex sea conditions, these rocking reduction devices will also meet various factors that affect the normal driving of the ship, so the optimized design of screw rocking reduction devices is of great significance for the safe driving of the ship in complex sea conditions [13]-[15].

In this study, an optimization design method of double gyro rocking reduction device based on nonlinear dynamics equations is proposed. Firstly, a ship-double gyro joint dynamics model considering nonlinear factors is established, and the irregular wave environment is accurately simulated using Torsethaugen wave spectrum. Then a PD approach controller based on transverse rocking angle feedback is designed to realize the accurate control of gyro approach. Finally, multi-objective optimization of the key parameters of the wave reduction gyro is carried out by genetic algorithm, which improves the wave reduction efficiency and reduces the quality and energy consumption

of the system at the same time. The validity of the proposed method is verified by Adams dynamics simulation and numerical calculation, which provides theoretical support and technical guidance for the engineering application of the dual gyro rocking reduction device.

II. Mathematical modeling

II. A.Gyro Decompression Device

The gyroscopic shock absorbing device can be divided into passive and active gyro stabilizers of 2 kinds. Passive gyro stabilizers are natural feed type, active gyro stabilizers are controller driven feed type. 2 ways of gyro stabilizers schematic shown in Figure 1.

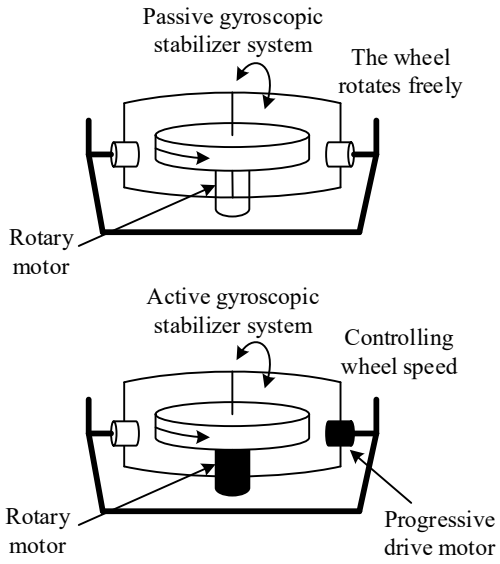

Figure 1: Schematic diagrams of two types of gyroscopic stabilizers

There are a number of problems with using only 1 gyro stabilizer to generate a transverse rocking motion to counteract torque. When the flywheel rotates around the inlet shaft, the direction of the gyro gimbal shaft changes, resulting in a change in the direction of the output torque of the gyro stabilizers, which generates unwanted torque and may lead to unwanted yawing or pitching motions of the ship [16]. To address this problem, the overall arrangement of the dual gyro stabilizers is shown in Fig. 2. 2 gyroscopic sway-reducing devices as 1 working group, with rotor speeds of equal magnitude and opposite direction, and rotor feeds of equal magnitude and opposite direction. This ensures that all torques generated in undesired directions will cancel each other out.

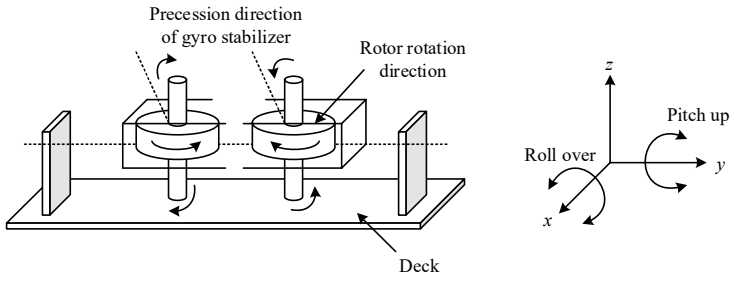

Figure 2: Overall layout of the dual gyroscope stabilizer

II. B.Dynamic modeling of a single gyro decoupling device

Before modeling the dynamics, a coordinate system is established. Let the carrier coordinate system or called the base coordinate system O-$\xi\eta\zeta$ of a single-frame control moment gyro be set up, with point O as the coordinate origin. Once the gyro decoupling stabilizer is installed on the ship, the ship becomes the base of the gyro stabilizer. The base coordinate system O-$\xi\eta\zeta$ rotates around the O axis α at an angle for the frame coordinate system O-xyz. The frame coordinate system O-xyz rotates around the Oz axis φ at an angle for the rotor coordinate system

O-$x_R y_R z_R$. The Oz axis is the rotor rotational axis, and the coordinate system O- xyz is used as the main axis coordinate system which is not involved in the rotor rotation. The linearized equation of motion of the gyro stabilizer with respect to the frame coordinate system O-xyz is expressed as:

$$\begin{cases} M_x = I_s \omega_s \dot{\alpha} \\ M_y = J\ddot{\alpha} - I_s \omega_s \dot{\phi} \cos\alpha \\ M_z = 0 \end{cases} \tag{1}$$

where, M_x, M_y and M_z are the gyroscopic moments around the corresponding axes, $N \cdot m$. ω_s is the rotational speed of the gyro wheel, r/s. α is the angle of advance, rad. J is the moment of inertia about the oy axis, kg·m². I_s is the polar moment of inertia of the gyro stabilizer, kg·m². ϕ is the angle of movement of the base with respect to the axis Oξ, i.e., the ship's transverse rocking angle, rad.

II. C.Joint ship and gyro dynamics model with dual gyro stabilizers

The nonlinear transverse rocking motion of a ship in waves is modeled, and the coupling effects of the ship's longitudinal rocking and first rocking motions as well as the transverse, longitudinal, and vertical rocking motions on the ship's transverse rocking are neglected:

$$(I_{44} + A_{44})\ddot{\phi} + B_{44}\dot{\phi} + C_{44}\phi = \tau_w \tag{2}$$

where, parameter I_{44} is the ship's transverse moment of inertia. The parameter A_{44} is the additional mass moment of inertia, kg·m². B_{44} is the transverse rocking damping kg·m²·s^{-1}. C_{44} is the transverse rocking restoring moment, N·m. The source term τ_w is the wave-generated transverse rocking moment, N·m.

Combining Eq. (1) and Eq. (2), the joint ship and gyro dynamics model for the dual gyro stabilizer is:

$$\begin{aligned} &(I_{44} + A_{44})\ddot{\phi} + B_{44}\dot{\phi} + C_{44}\phi = \tau_w - nI_s\omega_s\dot{\alpha}\cos\alpha \\ &I_1\ddot{\alpha} + B_g\dot{\alpha} + C_g\sin\alpha = I_s\omega_s\dot{\phi}\cos\alpha + \tau_c \end{aligned} \tag{3}$$

where I_s is the polar moment of inertia of the gyro stabilizer, kg·m². I_t is the transverse moment of inertia, kg·m². B_g is the gyro damping, kg·m²·s^{-1}. C_g is the gyro restoring moment, N·m. ω_s is the rotational speed, r/s. The source term τ_c is the control moment generated by the gyro-stabilizer, N·m. For a dual gyro-stabilizer n=2, $K_g = I_s\omega_s$ is the angular momentum generated by the gyro-deceleration device at the spin axis, kg·m²· s^{-1}.

If the incoming angular amplitude of the gyroscope $|\alpha|$ is small, Eq. (3) can be further linearized and expressed in state-space form:

$$\dot{x} = Ax + B_1 w + B_2 u, x = (\phi\alpha\dot{\phi}\dot{\alpha})^T \tag{4}$$

$$A = \begin{pmatrix} 0 & 0 & 1 & 0 \\ 0 & 0 & 0 & 1 \\ -\dfrac{C_{44}}{I_{44}+A_{44}} & 0 & \dfrac{B_{44}}{I_{44}+A_{44}} & \dfrac{2I_s\omega}{I_{44}+A_{44}} \\ 0 & -\dfrac{C_g}{I_i} & \dfrac{I_s\omega}{I_i} & \dfrac{B_g}{I_i} \end{pmatrix} B_1 = \begin{pmatrix} 0 \\ 0 \\ 0 \\ \dfrac{1}{I_{44}+A_{44}} \\ 0 \end{pmatrix} B_2 = \begin{pmatrix} 0 \\ 0 \\ 0 \\ 0 \\ \dfrac{1}{I_i} \end{pmatrix} \tag{5}$$

After establishing a joint ship and gyro dynamics model with dual gyro stabilizers, a gyro stabilizer PD inlet controller based on transverse rocking angle feedback is designed:

$$\tau_p = -K_p\phi - K_d\dot{\phi} \tag{6}$$

where, K_p represents the proportional controller coefficients. K_d represents the differential controller coefficients.

II. D.Wave force model

The modeling approach for wave disturbance effects in this paper uses a linear state space model. This approach is used in the control system mainly for testing system robustness and closed-loop control system performance analysis. Before calculating the irregular wave force and the ship motion response under irregular wave action, the wave spectrum $S(\omega)$ is determined. In this paper, the Torsethaugen wave spectrum is used to model irregular wave conditions.

In this model, the sea state is categorized into 2 types depending on the origin of the highest spectral peak, and the spectrum has 1 peak or 2 peaks, depending on the value of the peak period T_p [17]. The distinction between wind-dominated and swell-dominated (fully developed waves) sea states is defined by the value of Tr:

$$T_{pf} = a_f H_s^{1/3}, a_f = 6.6 \tag{7}$$

If $T_p < T_{pf}$, a wind-dominated sea state. If $T_p > T_{pf}$, the main spectral peak corresponds to a surge-dominated sea state system. If the value of T_{pf} is in the neighborhood of T_p, 2 spectral peaks are generated.

Based on the magnitude of the effect of the 2 spectra, the Torsethauger spectrum is calculated as follows:

$$\begin{gathered} S(\omega) = \sum_{j=1}^{2} E_j S_j(\omega), E_j = \frac{1}{16} H_y^2 T_{py} \\ S_1(\omega) = G_0 A_\gamma \omega^{-4} e^{-\omega^{-4}} \gamma^{e^{-0.5\sigma^2\omega^{-2}}}, S_2(\omega) = G_0 \omega^{-4} e^{-\omega^{-4}} \end{gathered} \tag{8}$$

The RAO is approximated by combining the linear ship's equations of motion as the adjustable gain $K \approx H_{ros}(s)H_v(s)$: where $H_{ros}(s)$ is the transfer function for the conversion of wave amplitude to wave-induced force, and $H_v(s)$ is the transfer function for the conversion of force to displacement, which is specifically treated as follows The gain adjustment is based on the final displacement $\eta w = KH(s)w(s)$ being within a practically acceptable range, $w(s)$ is Gaussian white noise, and $H(s)$ is the wave spectrum fitting transfer function. The second-order damped transfer function $H(s)$ that fits the wave spectrum function is as follows:

$$H(s) = \frac{2\lambda\omega_0\sigma s}{s^2 + 2\lambda\omega_0 s + \omega_0^2} \tag{9}$$

where, λ is the damping coefficient. ω_0 is the main frequency of the wave, s^-1, which is the peak frequency. The σ is a constant representing the wave energy.

Transform Eq. (9) into equation of state form:

$$\begin{cases} \dot{x}_w = A_w x_w + B_w w \\ y_w = c_w^T x_w \end{cases} \tag{10}$$

To wit:

$$\begin{cases} \begin{bmatrix} \tilde{x}_{w1} \\ \dot{x}_{w2} \end{bmatrix} = \begin{bmatrix} 0 & 1 \\ -\omega_0^2 & -\lambda\omega_0 \end{bmatrix} \begin{bmatrix} x_{w1} \\ x_{w2} \end{bmatrix} + \begin{bmatrix} 0 \\ K_w \end{bmatrix} w \\ y_w = \begin{bmatrix} 0 & 1 \end{bmatrix} \begin{bmatrix} x_{w1} \\ x_{w2} \end{bmatrix} \end{cases} \tag{11}$$

where x_w is the equation of state and x_{w2} is the first order derivative of x_{w1}. y_w is the output. w is zero-mean white noise. A_w is the state matrix. B_w is the control matrix. c_w^T is the observation matrix.

II. E.Simulation and Analysis

On the basis of SolidWorks 3D modeling, the assembly is saved as parasolid (*.x_t) format and imported into Adams.Adams software uses an interactive graphic environment and part libraries, constraint libraries, and force libraries to create a fully parametric geometric model of the mechanical system, and its solver adopts the Lagrangian equations method in the dynamics theory of the multi-rigid-body system to build the The system dynamics equations

are used to analyze the virtual mechanical system statically, kinematically and dynamically, and output the displacement, velocity, acceleration and reaction force curves.

The wave model can be divided into two-dimensional long peaked wave stochastic wave model and three-dimensional irregular short peaked wave stochastic wave model. Two-dimensional long-crested random waves, also known as binary irregular waves or long-crested waves, are waves that propagate in a definite direction with peaks and troughs parallel to each other and perpendicular to the direction of wave advancement. Three-dimensional irregular short-peaked random waves are waves generated by wind excitation, and due to the randomness of the wind direction, their waves will not only propagate in one direction, but also propagate in other directions, thus forming a mound of varying sizes on the surface of the sea, which is also referred to as ternary irregular waves or short-peaked waves. In this paper, binary irregular wave simulation is used to study the dynamic characteristics of ships in random waves. The long wind waveform can be approximated as a sine function image form. The sine function A*sin(Bd*time) is used to simulate the period and size of the wave, where A refers to the amplitude of the wave, and B refers to the distance moved by the wave per unit time on the x-axis, i.e., the period. Waves at sea are actually irregular, they consist of a variety of waves with different wavelengths, wave heights and steepness. Observed statistics show that: 1/10 of the wave height is twice the average wave height, which is called the maximum wave height (hw/10). 1/3 of the wave height is 1.6 times the average wave height, which is called the trinity average wave height or meaningful wave height (hw/3). The wave heights that people visually observe at sea are very close to the meaningful wave heights. In order to make the simulation more convenient and targeted, in order to simulate the waves more accurately and conveniently, this paper takes the meaningful wave height to simulate different levels of waves. In the case of 0 r/min and 8000 r/min rotor speed of the gyro decoupling system respectively, the Adams dynamics simulation is carried out for different levels of waves, and the simulation time is set to 10 s, and the number of simulation steps is set to 5000. The simulation results of the waves of level 1~3 are shown in Figs. 3~5, respectively (Figs. a and b are the simulation results of the waves of level 0 r/min and 8000 r/min, respectively). According to the simulation results, it can be seen that: when the wave level is less than three, the marine gyroscope designed in this paper has a very good function of transverse rocking reduction, and the rocking reduction performance can even reach about 90% in the first level of waves. Marine gyroscope anti-transverse rocking ability and rotor position relative to the rotor axis, that is, and the rotational inertia. The gyro rotor in this test has a small mass, so the rocking reduction ability is limited, and when a larger rotor is used, the rocking reduction ability will be enhanced. At the same time, the factors affecting the rotation speed of the rotor can be reduced and the rotation speed of the rotor can be increased, for example, the gyro rotor can be made to rotate in a vacuum-enclosed environment, which can increase the rotor speed by more than two times, the weight can be reduced by one-third, and the power consumption is only one-half of the past. According to the simulation results, two obvious weaknesses of this test device can be found: 1) the moment of opening the rocking reduction device, it will cause an effect similar to the rapid shaking of the ship; 2) when the wave level is too large, the gyro rocking reduction device not only does not reduce the rocking, but even enhances the ship's transverse rocking. For this phenomenon, a controller can be added to the rocking reduction system to control the gyro-rocking reduction device, so that it can realize the active control of the movement when it is subjected to external moments, thus reducing the rocking.

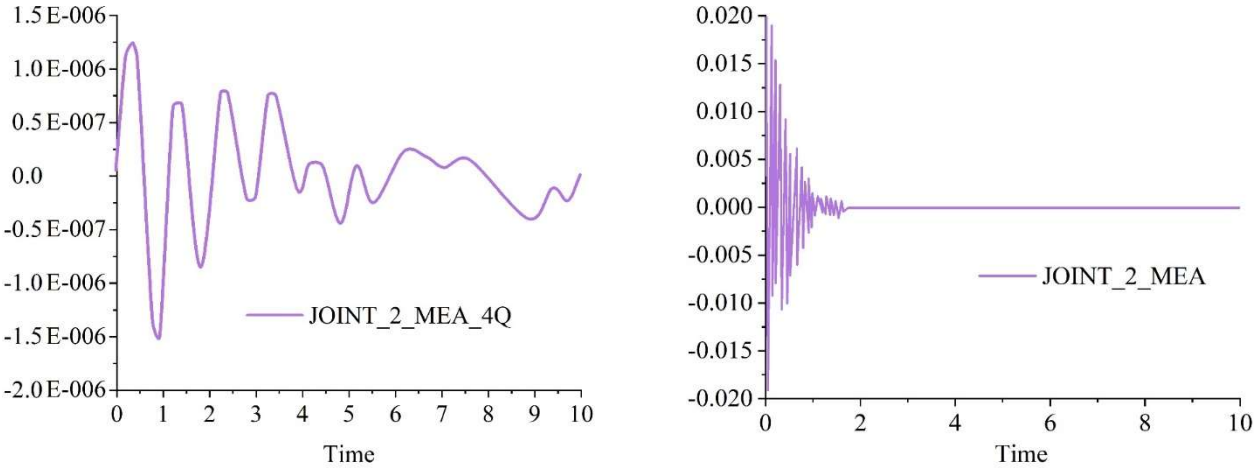

(a) 0 r/min simulation results (b) 8000 r/min simulation results

Figure 3: First level wave simulation results

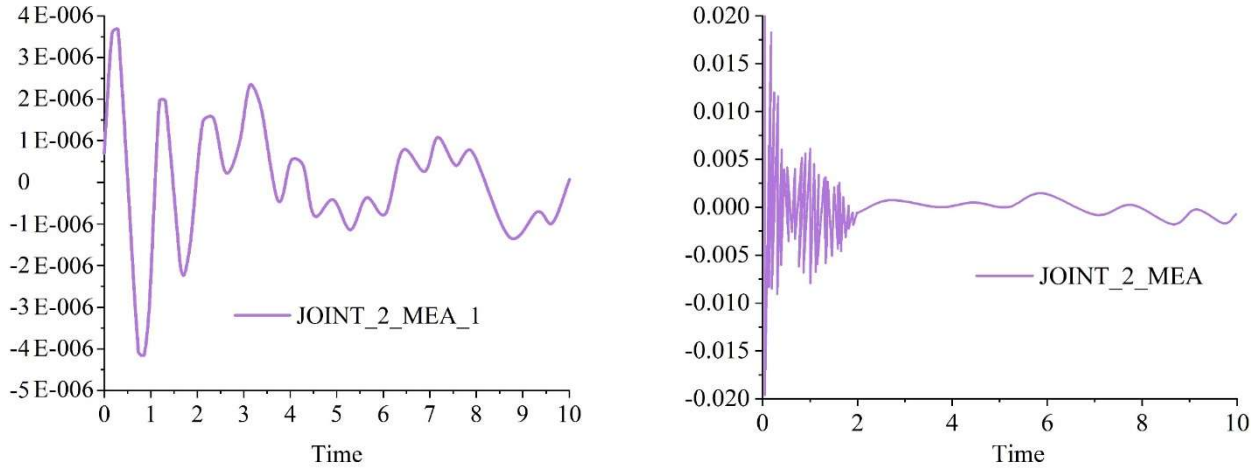

(a) 0 r/min simulation results (b) 8000 r/min simulation results

Figure 4: Secondary wave simulation results

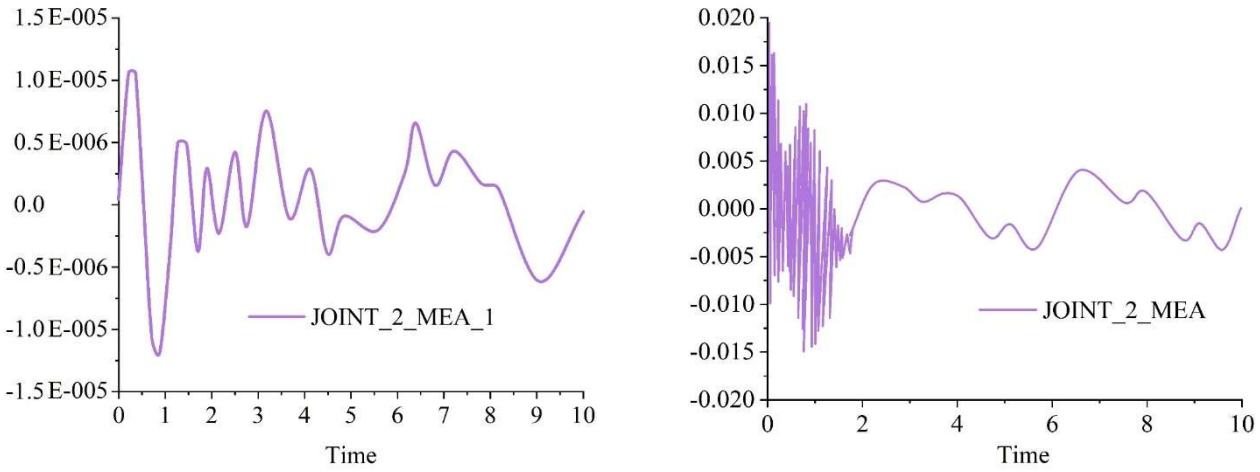

(a) 0 r/min simulation results (b) 8000 r/min simulation results

Figure 5: Three level wave simulation results

III. Optimization method of damping parameter of decoupling gyroscope based on genetic algorithm

According to the shaking gyro dynamics model, when the feed angle reaches 90 °, the output shaking moment is 0, at this time, the shaking effect of the gyro disappears, that is, it enters the singular state, therefore, in the actual engineering applications, generally through the mechanical limit will be shaking the gyro's feed angle is limited to ± 70 ° or less, and at the same time, in the direction of the gyro's feed axis to apply damping moment in order to prevent the gyro energy premature exhaustion. In addition, different sea state, ship structure and gyro structure will lead to changes in the gyro's inlet characteristics, which makes it difficult to achieve the best rocking reduction effect. Therefore, based on different application scenarios, it is necessary to optimize the passive control parameters of the rocking reduction gyro, taking into account the specific parameters of the ship and the gyro's angular momentum and other constraints. Commonly used optimization algorithms include ant colony algorithm, genetic algorithm, particle swarm algorithm, etc. In this paper, we will use genetic algorithm to optimize the damping coefficient of the rocking reduction gyro.

III. A. Genetic algorithms

First, the damping coefficient-decoupling efficiency relationship is established under different sea states. Then, the evolutionary operations such as selection, crossover and mutation are used to continuously optimize the feed damping coefficient, and the optimal solution is finally derived. The optimization flow of the rocking reduction gyro advance control based on genetic algorithm is shown in Fig. 6.

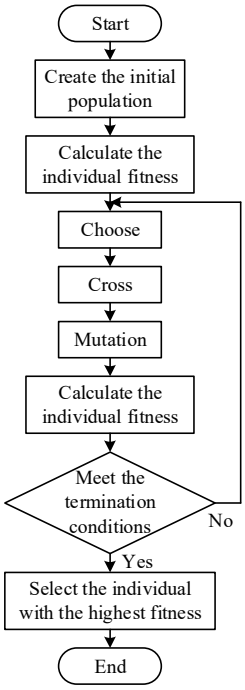

Figure 6: Optimization process of the genetic algorithm

III. B. Adaptation function design

In practical engineering applications, the statistical value of the transverse rocking angle sequence over a period of time is generally used as a parameter to measure the intensity of the ship's transverse rocking, which is defined as the mean value of the first 1/3 of the data in the descending order of the transverse rocking angle sequence. In this paper, a nonlinear transverse rocking-deceleration gyro joint dynamics model of the ship is constructed by Matlab/Simulink, and due to the existence of nonlinear terms in the system, it is necessary to use the fourth-order Runge-Kutta method to find the numerical solution, so as to get the sequence of transverse rocking angles of the ship within the set interval, and then compute the transverse rocking angle trinity value. The core content of the genetic algorithm is the design of the fitness function [18]. In this paper, the choice of damping coefficient of the rocking reduction gyro is a contradictory problem, if the damping coefficient is small, the rocking reduction efficiency is high, but it is easy to cause the jittering of the inlet damping system, and ultimately it is impossible to realize the precise control. If the damping coefficient is large, although the vibration of the inlet damping system can disappear, it will affect the shaking reduction efficiency, so how to balance between the shaking reduction efficiency and the vibration of the inlet system is the key problem to be solved in this paper.

When measuring the feed angle sequence, the signal spectrum $S_\beta(\omega)$ can be obtained by Fast Fourier Transform, and then the area of the envelope of the high-frequency component curve A_{fH} is utilized to measure the degree of vibration jittering of the feed damping system.

According to the working principle of shaking reduction gyro, the shaking reduction efficiency is highest when its inlet frequency is consistent with the ship's transverse rocking frequency. The ship's transverse rocking frequency depends on the waves and its intrinsic transverse rocking frequency, which is usually lower than 1Hz, so this paper sets the high-frequency component frequency interval $[f_L, f_H]$=1~5Hz, and takes the sampling frequency f_s =100Hz, so that the envelope area of the high-frequency component curve is:

$$A_{fH} = \int_{f_L}^{f_H} S_\beta(\omega) d\omega \tag{12}$$

where f_L, f_H are the lower and upper frequency limits of the high-frequency component, respectively.

The shaking reduction efficiency η_ϕ is calculated as:

$$\eta_\phi = \frac{\overline{\phi_N} - \overline{\phi_P}}{\overline{\phi_N}} \times 100\% \tag{13}$$

where $\overline{\phi_N}, \overline{\phi_P}$ are the trinity values of the ship's transverse rocking after the rocking reduction is turned off and on, respectively.

The two optimization objectives of this paper are 1) the highest rocking reduction efficiency, and 2) the smallest vibration shaking degree of the inlet damping, whose weight coefficients are α_1 and α_2, respectively. Based on the optimization objective function, the genetic algorithm fitness function is described as follows:

$$\begin{cases} (I_{xx}+J_{xx})\ddot{\phi}_N + c_1\dot{\phi}_N + c_3\dot{\phi}_N^3 + k_5\phi_N^5 = Dh\alpha(t) \\ (I_{xx}+J_{xx})\ddot{\phi}_P + c_1\dot{\phi}_P + c_3\dot{\phi}_P^3 + k_5\phi_P^5 = Dh\alpha(t) - h_0\dot{\beta}\cos(\beta) \\ J\ddot{\beta} = h_0\dot{\phi}_P\cos(\beta) - C_m I \\ L\dot{I} = U_{d0} - RI - C_m\dot{\beta} \\ U_{d0} = \mu r\dot{\beta} \\ \eta_\phi = \dfrac{\overline{\phi_N} - \overline{\phi_P}}{\overline{\phi_N}} \\ \max\left\{ J_{OP} = \alpha_1\overline{\eta_\phi} + \alpha_2\left(\dfrac{1}{A_{HI}}\right)\right\} \\ s.t.\begin{cases} -1.22 < \beta < 1.22 \\ 10 < r < 120 \end{cases} \end{cases} \tag{14}$$

Based on Eq., a functional relationship can be constructed between the gyro-advancement damping coefficient r and the optimization objective J_{op}, and the parameter optimization is carried out through the genetic algorithm until the optimal damping coefficient r^* is found. Considering the influence of the actual sea state, in order to prevent the deceleration gyro from entering the singular state, the deceleration gyro feed angle β is limited to between ±70°, i.e., between ±1.22 rad. At the same time, according to the mechanical characteristics of the feed damping motor, the damping coefficient r applied to the feed shaft should be limited to between 10 and 120.

IV. Simulation tests and analysis of results

IV. A. Comparative analysis before and after optimization based on shaking reduction effect

Considering only the first objective function, the shaking reduction effect rate as the objective function, in the MATLAB simulation software through the bacterial foraging optimization algorithm for optimization solution, the first objective optimization calculation curve is shown in Figure 7, the objective function of the shaking reduction rate from the initial 72.22% to 80%, and at the same time to get the optimized shaking reduction gyroscope parameter values, the first objective of the parameters of the value of before and after the optimization of the comparison is shown in Table 1. From the table, it can be seen that: the inner diameter of the gyro rotor becomes larger, the outer diameter is slightly smaller, the length of the rotor shaft becomes smaller, and the speed of the motor is changed to the highest speed, which causes the rotating momentum moment of the gyro to increase, i.e., the rocking reduction rate is increased. The thickness of the gyro rotor is slightly reduced, which causes the gyro's inward momentum moment to decrease, i.e., the rocking reduction rate decreases. The damping coefficient is the intermediate value, which is the optimal value of damping coefficient, at which the ship has the highest rocking reduction rate. Comparison of transverse rocking angle before and after the first objective optimization is shown in Fig. 8, the fluctuation amplitude of transverse rocking angle has decreased significantly, the rocking reduction effect has been greatly improved, the rocking reduction rate is increased from 71.5% to 80%, and the overall mass of rotor is also decreased, from the original 2526kg to 2043kg.

Table 1: The first target is optimized before and after the optimization of the parameters

	Inner diameter D_1/m	Outside diameter D_2/m	Shaft diameter D_3/m	Thickness H_1/m
Before optimization	1.068	1.236	0.177	0.697
After optimization	1.105	1.235	0.172	0.613
	Axis length H2/m	Floor thickness H3/m	Damping coefficient/m	Speed of revolution ϖ / r / min
Before optimization	1.043	0.057	25360	1235
After optimization	0.852	0.0469	27165	1302

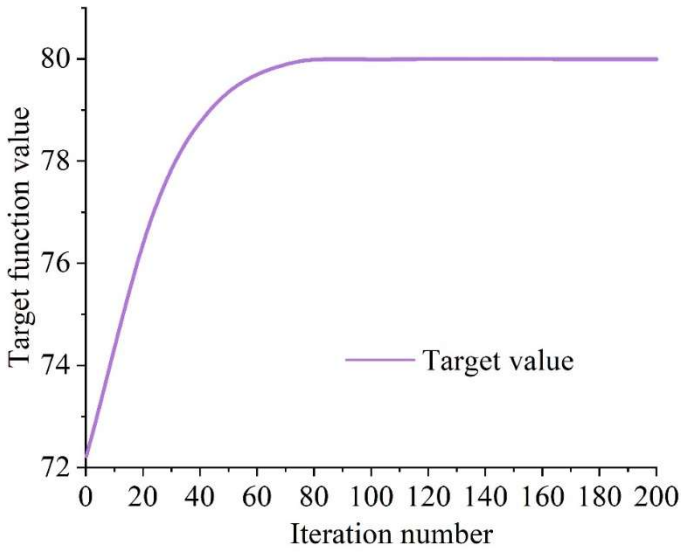

Figure 7: First target optimization calculation curve

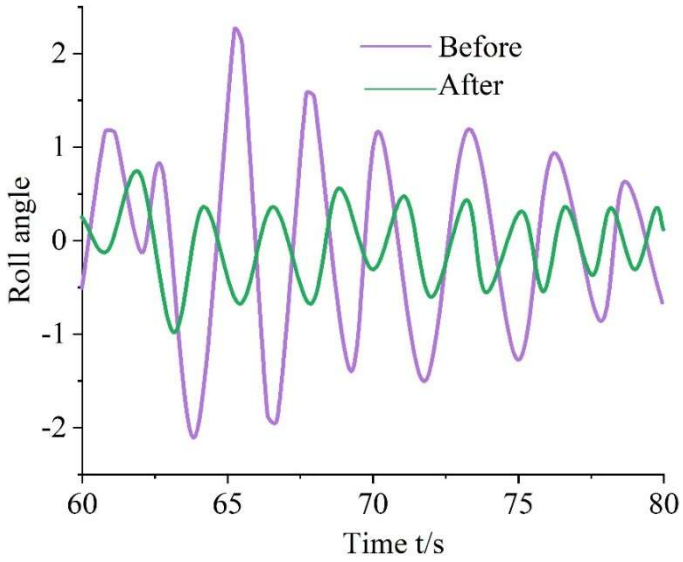

Figure 8: Comparison of roll angle before and after optimization of the first target

IV. B. Comparative analysis before and after optimization based on lightweighting

Considering only the second objective function, i.e., the rotor mass as the objective function, the optimization solution is carried out by the bacterial foraging optimization algorithm in MATLAB simulation software, and the optimization calculation curve of the second objective is shown in Fig. 9, and the rotor mass of the objective function is reduced from the initial 2,526 kg to 1,491 kg. Comparison of the values of each parameter of the second objective before and after the optimization is shown in Table 2. From the table, it can be seen that: the inner diameter of the gyro rotor becomes larger, the outer diameter increases to the upper limit, the length of the rotor shaft decreases to the lower limit, and the rotational speed of the motor changes to the highest, which causes the rotational momentum moment of the gyro to increase, and then increase the rocking reduction rate. The thickness of the gyro rotor is reduced significantly to the lower limit, causing the gyro's inlet momentum moment to decrease, which reduces the rocking reduction rate appropriately, but drastically reduces the rotor mass. The damping coefficient is increased to the middle value of the constraints, which is the optimal value of the damping coefficient, and the ship has the highest rocking reduction rate at this coefficient. The changes in all parameters are in line with the conclusions of the ship rocking reduction gyroscope characterization study in Chapter 3. Comparison of transverse rocking angle before and after the optimization of the second objective is shown in Fig. 10, the fluctuation of transverse rocking angle decreases, but the rocking reduction effect is not much improved from 73.2% to 75.1%, but the rotor mass decreases obviously from the original 2526kg to 1492kg.

Table 2: Comparison of the parameters of the second target before and after optimization

	Inner diameter D_1/m	Outside diameter D_2/m	Shaft diameter D_3/m	Thickness H_1/m
Before optimization	1.06	1.24	0.19	0.68
After optimization	1.15	1.2827	0.14	0.45
	Axis length H2/m	Floor thickness H3/m	Damping coefficient/m	Speed of revolution ϖ / r / min
Before optimization	1.02	0.09	25306	1263
After optimization	0.84	0.0565	27493	1312

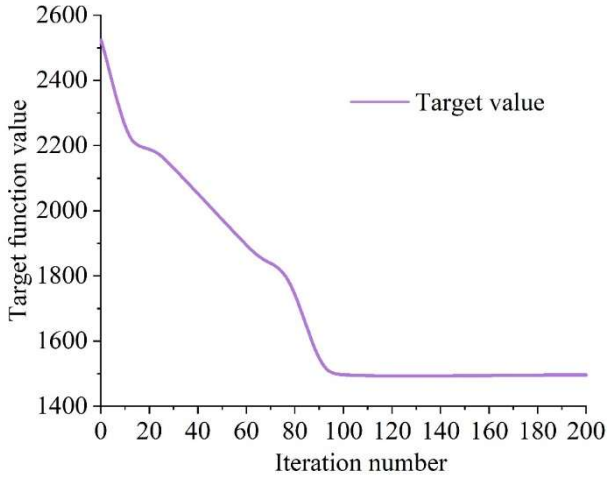

Figure 9: Second target optimization calculation curve

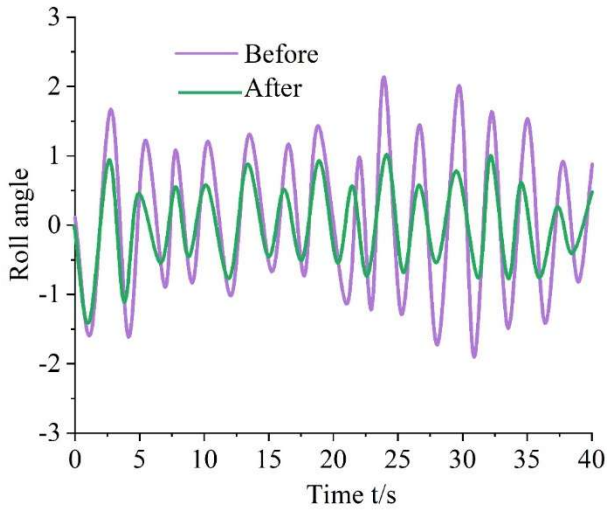

Figure 10: Comparison of roll angle before and after optimization of the second target

IV. C. Comparative analysis before and after optimization based on power drive

Consider only the third objective function, that is, the power drive as the objective function, in the MATLAB simulation software through the bacterial foraging optimization algorithm for the optimization of the solution, the third objective optimization calculation curve is shown in Figure 11, the objective function of the motor speed from the initial 1251 to the optimizable minimum value of 1063, the third objective of the various parameters before and after the optimization of the value of the comparison is shown in Table 3. From the table can be seen: the gyro rotor inner diameter and outer diameter slightly increased, the length of the rotor shaft is reduced, the motor speed is reduced to the minimum, causing the gyro's rotating momentum moment is reduced, that is, the rocking reduction rate is reduced. The thickness of the gyro rotor is slightly reduced, causing the gyro's inlet momentum moment to decrease, although it will appropriately reduce the rocking reduction rate, but reduces the rotor mass. The damping coefficient increases to the middle value of the constraints, which is the optimal value of the damping coefficient, and the ship has the highest rocking reduction rate under this coefficient. Comparison of transverse rocking angle before and

after the third objective optimization is shown in Fig. 12, the fluctuation amplitude of transverse rocking angle is improved, and the reduction of rocking reduction effect is not obvious, from 73.1% to 72.5%, but the mass of the rotor is improved, from the original 2526kg to 2529kg.

Table 3: Comparison of the parameters of the third target before and after optimization

	Inner diameter D_1/m	Outside diameter D_2/m	Shaft diameter D_3/m	Thickness H_1/m
Before optimization	1.0663	1.2398	0.1819	0.6985
After optimization	1.0895	1.2692	0.1554	0.6276
	Axis length H2/m	Floor thickness H3/m	Damping coefficient/m	Speed of revolution ϖ / r / min
Before optimization	1.0433	0.0486	25305	1236
After optimization	0.8996	0.0509	26712	1122

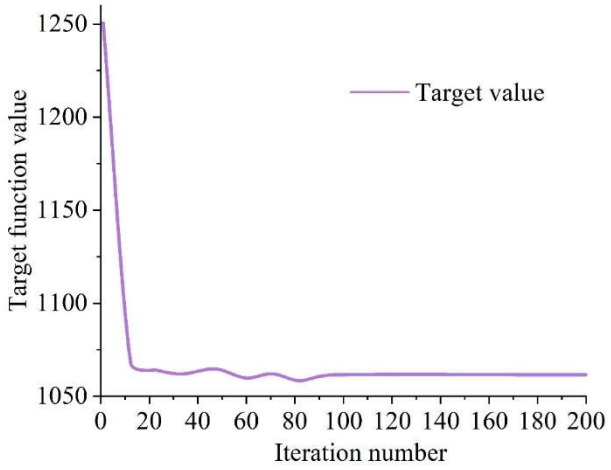

Figure 11: The third goal optimizes the calculation curve

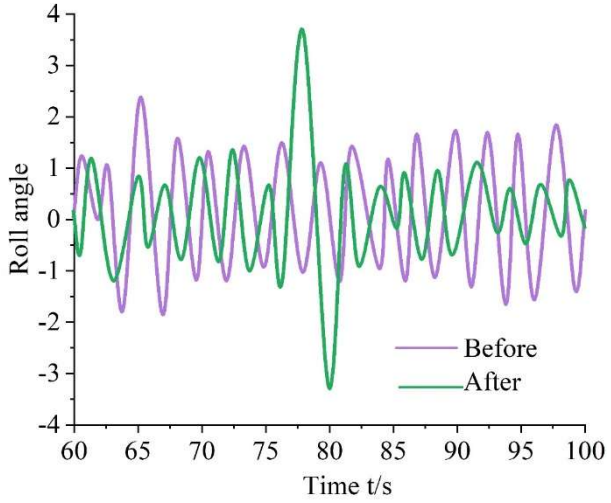

Figure 12: Comparison of roll angle before and after optimization of the third target

IV. D. Comparative analysis before and after multi-objective based optimization

The multi-objective optimization calculation curve is shown in Fig. 13, and the objective function value is reduced from 740.1 to 532.5. A comparison of the multi-objective parameter values before and after optimization is shown in Table 4. From the table, it can be seen that: the inner diameter and outer diameter of the gyro rotor are slightly increased, the length of the rotor shaft is reduced, and the rotational speed of the motor is slightly increased, which causes the rotational momentum moment of the gyro to be slightly increased, i.e., a small increase in the rocking reduction rate. The thickness of the gyro rotor is slightly reduced, causing the gyro's inward momentum moment to decrease, although it will appropriately reduce the rocking reduction rate, but reduces the rotor mass. The damping

coefficient increases to the middle value of the constraints, which is the optimal value of the damping coefficient, and the ship has the highest rocking reduction rate under this coefficient. Comparison of transverse rocking angle before and after multi-objective optimization is shown in Fig. 14, the fluctuation amplitude of transverse rocking angle is reduced, the rocking reduction effect is slightly improved from 71.46% to 75.34%, and the mass of the rotor is reduced, from the original 2526kg to 2165kg.

Table 4: The multi-objective parameters are compared before and after the optimization

	Inner diameter D_1/m	Outside diameter D_2/m	Shaft diameter D_3/m	Thickness H_1/m
Before optimization	1.0696	1.2398	0.1788	0.7034
After optimization	1.1123	1.2551	0.1624	0.6076
	Axis length H2/m	Floor thickness H3/m	Damping coefficient/m	Speed of revolution ϖ / r / min
Before optimization	1.05	0.0492	25361	1236
After optimization	0.8406	0.0598	26742	1228

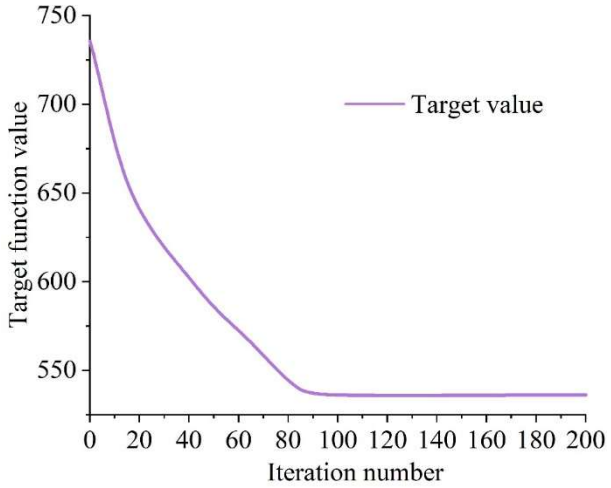

Figure 13: Multi-objective optimization calculation curve

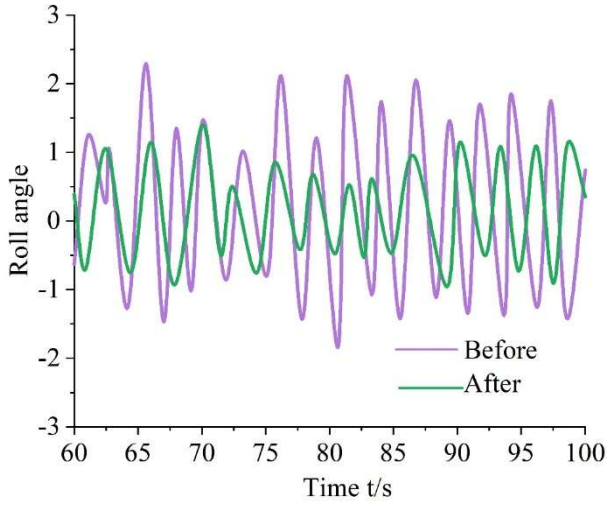

Figure 14: Comparison of roll angle before and after multi-objective optimization

V. Conclusion

This study has successfully solved the key technical problem of transverse rocking control for ships under complex sea conditions by establishing the optimization design method of double gyro rocking reduction device based on nonlinear dynamic equations. The dual gyro rocking reduction system effectively avoids the yaw and pitch problems caused by the single gyro system through the design concept of mutual offsetting of undesirable torque. Adams

dynamics simulation results confirm that the device performs well in low-grade waves, and the rocking reduction performance can reach 90% under the first-level wave conditions, which is significantly better than that of the traditional rocking reduction methods.

The application of genetic algorithm optimization strategy realizes the multi-objective coordinated optimization of the rocking reduction system. The single wave reduction optimization results in a significant increase in the system performance from 72.22% to 80%, and the rotor mass is reduced from 2526 kg to 2043 kg, which achieves the dual objectives of performance and lightweighting. The lightweighting optimization significantly reduces the rotor mass to 1491kg, which creates favorable conditions for the engineering application of the system. The multi-objective comprehensive optimization achieves the best compromise in terms of shaking reduction effect, mass control and energy consumption balance, with the shaking reduction rate increased to 75.34% and the mass controlled at 2165kg, which reflects the effectiveness of the optimization algorithm.

The nonlinear dynamics modeling method accurately describes the ship's motion characteristics under complex sea conditions, and the introduction of Torsethaugen wave spectrum makes the simulation closer to the actual marine environment. The design of PD inlet controller realizes the precise control of gyro inlet, which effectively prevents the system from entering into the singular state. This research result provides a complete theoretical framework and technical scheme for the engineering application of dual gyro rocking reduction device, which is of great significance to enhance the safety and comfort of the ship under severe sea conditions.

References

[1] Enin, S. S., Omelchenko, E. Y., & Beliy, A. V. (2018, May). Crane anti-sway control system with sway angle feedback. In 2018 International Conference on Industrial Engineering, Applications and Manufacturing (ICIEAM) (pp. 1-5). IEEE.

[2] Caporali, R. P. (2023). Anti-sway method for reducing vibrations on a tower crane structure. International Journal of Nonlinear Sciences and Numerical Simulation, 24(1), 171-184.

[3] Chen, J., Ma, J., & Lo, S. (2016). Modelling pedestrian evacuation movement on a swaying ship. In Traffic and Granular Flow'15 (pp. 297-304). Springer International Publishing.

[4] Zheng, X., Zhang, J., & Zhou, C. (2018). Effect of ship swaying and process parameters on extrusionpeeling of Antarctic krill. Transactions of the Chinese Society of Agricultural Engineering, 34(1), 273-278.

[5] Sun, H., Wang, C., & Pang, W. (2019). Modeling and simulation of ship swaying attitude based on linear system theory. In Complex, Intelligent, and Software Intensive Systems: Proceedings of the 12th International Conference on Complex, Intelligent, and Software Intensive Systems (CISIS-2018) (pp. 695-703). Springer International Publishing.

[6] Cheng, M. J., Jiang, W. J., Tao, B. W., Zheng, X. T., & Guo, L. X. (2021, December). Influence of Ship Swaying motion on performance of Maritime Laser Communications in the Turbulence. In 2021 13th International Symposium on Antennas, Propagation and EM Theory (ISAPE) (pp. 1-3). IEEE.

[7] Dan, Q., Xiaogang, C., Jinhui, H., & Chao, Z. (2019, March). Study on the method of ship swaying isolation in the ship's radar digital guidance manner. In 2019 IEEE 3rd Information Technology, Networking, Electronic and Automation Control Conference (ITNEC) (pp. 1799-1803). IEEE.

[8] Lv, Z., Liu, P., Ning, D., & Wang, S. (2024). Anti-Swaying Control Strategy of Ship-Mounted 3-RCU Parallel Platform Based on Dynamic Gravity Compensation. Machines, 12(3), 209.

[9] Li, X., Mei, Z., Zhu, D., & Xie, B. (2017). Modeling and anti-sway control of ship-mounted crane. Advances in Mechanical Engineering, 9(9), 1687814017727252.

[10] Liu, X. J., Fan, S. M., Wang, J. H., & Wan, D. C. (2015, June). Hydrodynamic simulation of pure sway tests with ship speed and water depth effects. In ISOPE International Ocean and Polar Engineering Conference (pp. ISOPE-I). ISOPE.

[11] Chen, C., Liu, Y. D., Zhang, W., He, Y. P., & Tang, Y. Y. (2023). Free roll decay simulation of a polar research vessel with an anti-roll tank based on CFD. Ocean Engineering, 285, 115429.

[12] Kapsenberg, G., & Carette, N. (2023). A consistent method to design and evaluate the performance of anti-roll tanks for ships. Ship Technology Research, 70(2), 117-145.

[13] Lee, D., Kim, S., Jung, J., & Kim, D. (2023, June). An application of anti-roll tank to reduce roll motion of containership. In ISOPE International Ocean and Polar Engineering Conference (pp. ISOPE-I). ISOPE.

[14] Li, B., Zhang, X., Wang, J., & Chen, N. (2022). Anti-roll characteristics of marine gyrostabilizer based on adaptive control and hydrodynamic simulation. Journal of Marine Science and Engineering, 10(1), 83.

[15] Subramanian, R., & Jyothish, P. V. (2020). Genetic algorithm based design optimization of a passive anti-roll tank in a sea going vessel. Ocean Engineering, 203, 107216.

[16] A. S. Meshchanov & L. A. Gataullina. (2018). Robust Control of a Gyroscopic Stabilizer at Sliding Modes. Russian Aeronautics,61(4),671-676.

[17] Yanqing Han ,Conghuan Le ,Puyang Zhang& Shengnan Xu. (2024). Comparisons of Wave Force Model Effects on the Structural Responses and Fatigue Loads of a Semi-Submersible Floating Wind Turbine. Journal of Ocean University of China,23(1),69-79.

[18] Yuanyuan Zhu,Shijie Su,Yuchen Qian,Yun Chen & Wenxian Tang. (2020). Parameter Optimization for Ship Antiroll Gyros. Applied Sciences,10(2).